



Removal of malachite green and methylene blue by $\text{Fe}_{0.01}\text{Ni}_{0.01}\text{Zn}_{0.98}\text{O}$ /polyacrylamide nanocomposite using coupled adsorption and photocatalysis



Shashi Kant^a, Deepak Pathania^b, Pardeep Singh^b,
Pooja Dhiman^c, Amit Kumar^{a,b,*}

^a Department of Chemistry, Himachal Pradesh University, Summer Hill, Shimla 171005, India

^b School of Chemistry, Shoolini University, Solan, Himachal Pradesh 173212, India

^c Department of Physics, Himachal Pradesh University, Summer Hill, Shimla 171005, India

ARTICLE INFO

Article history:

Received 30 June 2013

Received in revised form 30 August 2013

Accepted 1 September 2013

Available online 8 September 2013

Keywords:

Nanocomposite

Adsorption

Solar light

Enhanced photocatalysis

Dye removal

ABSTRACT

This study describes the removal of malachite green (MG) and methylene blue (MB) from aqueous solution using adsorption and photodegradation activity of $\text{Fe}_{0.01}\text{Ni}_{0.01}\text{Zn}_{0.98}\text{O}$ /polyacrylamide nanocomposite (FNZP/PAM). Fourier transform infra red spectroscopy (FTIR), X-ray diffraction (XRD), scanning electron microscopy (SEM), energy dispersive X-ray (EDX), high resolution transmission electron microscopy (HRTEM), small area electron diffraction (SAED) and UV-vis spectroscopy techniques were used for characterization of nanocomposite. The coupled photocatalysis and adsorption shown by FNZP/PAM resulted in fast and higher degradation of MB and MG as compared to dye removal by FNZP. The FNZP/PAM shows a higher rate of dyes removal due to excellent adsorbing properties of cross linked polyacrylamide (PAM). A remarkable 97.56% of MB and 96.13% of MG was achieved for FNZP/PAM by coupled adsorption and photocatalysis after two hours. Thermo gravimetric analysis confirmed the higher thermal stability of FNZP/PAM as compared to PAM. The nanocomposite proved to be a promising antimicrobial agent against bacterial strains of *Staphylococcus aureus* (*S. aureus*).

© 2013 Elsevier B.V. All rights reserved.

1. Introduction

The recent population explosion has lead to rapid proliferation of industries and hence environmental pollution. Textile industries discharge large amounts dyes into water, some of which are mutagenic and carcinogenic to human beings [1]. The dye effluents are characterized by their fluctuating pH with suspended particles, high oxygen demand, non-biodegradability and stability to many oxidizing agents [2,3].

Most dyes have complex structures and their high recalcitrance to degradation is a great challenge for decolorisation and complete mineralization. Major research has been undertaken to develop new promising materials for dye removal. Malachite green ($\text{C}_{23}\text{H}_{25}\text{N}_2\text{Cl}$, C. I. No. 42000) is a green crystal powder with lustre, highly soluble in water [4]. It acts as a respiratory enzyme poison in fish. It decreases food intake, causes damage to liver, kidney and is infectious to skin, eyes and bones. Methylene blue ($\text{C}_{16}\text{H}_{18}\text{N}_3\text{SCl}$,

C. I. No. 52015) causes nausea, hypertension, haemolysis and respiratory distress.

Due to different problems caused by various conventional dye removal agents, there has been a strong interest in organic-inorganic composites with nano scale dimensions. They find numerous potential applications such as enhancement conductivity [5,6], toughness [7], optical activity [8,9], catalytic activity [10], and chemical selectivity [11]. In these materials, inorganic and organic components are mixed or hybridized at nanometer scale with virtually any composition leading to the formation of hybrid/nanocomposite materials [12–16]. Metal oxide nanoparticles have broad applications in the manufacture of both the commercial and personal products. At present various inorganic metal oxides nanoparticles are being synthesized but ZnO nanomaterials have attracted great interest because of their unique and fascinating optical, electrical, mechanical, and piezoelectric properties. ZnO has wide use in fundamental research and potential applications in hydrogen-storage [17], field emitters [18], gas sensors [19], ultraviolet lasers [20], solar cells [21], piezoelectric devices [22] and photocatalysts [23].

The various techniques which have been extensively used for dye removal are coagulation, chemical oxidation, adsorption, microbial degradation and photocatalysis [24,25]. The two most

* Corresponding author at: School of Chemistry, Shoolini University, Solan, Himachal Pradesh 173212, India. Tel.: +91 177 2830944/9625310313.

E-mail address: mittuchem83@gmail.com (A. Kumar).

reliable and effective methods for removal of organic dyes are adsorption and heterogeneous photocatalysis. Adsorption is one of effective methods with high efficiency and no harmful by products. But adsorption transfers pollutants merely from one medium to other rather than their degradation [26]. Since the first pioneering papers in the seventies, the interest of scientists in heterogeneous photocatalysis has grown very much and thousands of papers have been published. This technology has been successfully applied to water splitting, hydrogen formation, dye sensitized cells production, environmental remediation by removal of organic and inorganic pollutants, inactivation/killing of bacteria, etc. Heterogeneous photocatalytic process leads to oxidation-reduction and finally to the overall degradation of a wide variety of organic pollutants through their interaction with photo generated holes or reactive oxygen species, such as $\cdot\text{OH}^-$ and $\cdot\text{O}_2^-$ radicals. The doping of zinc oxide by transition metals has a pronounced effect on its photocatalytic efficiency. ZnO nanoparticles can be excited by UV light to produce electron hole pairs. To improve the photoactivity of ZnO, the absorption of light in the visible light spectrum must be enhanced (visible light forms approximately 43% of the solar spectrum). If this enhancement is achieved ZnO nanoparticles would be more applicable in the environmental applications using sunlight. Ullah and Dutta [27] studied the photocatalytic degradation of methylene blue in presence of manganese doped ZnO and achieved better results than undoped one. Wang et al. [28] investigated the applicability of Ag doped ZnO nanocrystals for removal of methylene blue. They found that doped sample enhanced the visible absorption and hence the degradation. He et al. [29] studied the effect of doping amount of Co doped ZnO nanopowders on the photodegradation of Rhodamine B. It was reported that Co doping decreased the photocatalytic efficiency of ZnO and lower the dopant concentration the amount better the photocatalyst.

The Fe doped ZnO studies by Zhang et al. [30] revealed that the ZnO/Fe nanowires performed even better than P-25 against Methyl orange. It has been reported by Xianghong et al. [31] that 2% Fe doped ZnO degraded methyl orange to 80.79% in 210 min of sunlight irradiation. Zhao et al. [32] explored 1%, 2% and 5% Ni doped ZnO nanocrystals for photocatalytic removal of Rhodamine. In this study 5% doped sample brings about highest degradation. From the above discussion, it can be inferred Fe and Ni have so far been explored for dye removal and have higher photocatalytic activity than bare ZnO. However, high dopant concentrations in case of Fe and moderate concentrations in case of Ni have been found more effective.

Recently, adsorption process has proven to be an effective and reliable method for dye removal. The major advantages of an adsorption treatment for the control of water pollution are less investment in terms of initial development cost, simple design, easy operations, free from generation of toxic substances, and easy and safe recovery of the adsorbent as well as adsorbate materials. Although adsorption is a widely exploited method for dye effluent treatment, it only transfers dye from aqueous to solid phase thus leading to secondary pollution. Cross linked polyacrylamide (PAM) is a superabsorbent polymer and a common flocculants for waste water treatment [33–35]. Advanced oxidation process initiated by photocatalytic degradation can offer a better solution for decolorization, breakdown and mineralization of dyes. The present work focuses on the coupling of both adsorption and photocatalysis phenomenon for efficient removal of Methylene blue and Malachite green form aqueous phase.

To the best of our knowledge, no study has been reported on the preparation of FNZP/PAM nanocomposite with photocatalytic activity. The precedent work deals with co-doping of ZnO using Fe and Ni as dopant in lower concentrations enhanced visible light activity. The visible light activity of FNZP/PAM will be exploited for the removal of MB and MG through coupled adsorption and

photocatalysis processes. The antibacterial activity of FNZP/PAM is evaluated against *S. aureus*.

2. Materials and methods

2.1. Materials

All the chemicals used were of analytical grade. Acrylamide, nickel nitrate, zinc nitrate, ferric nitrate, ammonium persulphate and *N,N'*-methylenebisacrylamide were procured from Merck India and used as such. Malachite green and methylene blue were purchased from Sigma-Aldrich.

2.2. Synthesis of $\text{Fe}_{0.01}\text{Ni}_{0.01}\text{Zn}_{0.98}\text{O}$ nanoparticles (FNZP)

For preparing the $\text{Fe}_{0.01}\text{Ni}_{0.01}\text{Zn}_{0.98}\text{O}$ nanoparticles, 11.652 g of zinc nitrate, 0.162 g of nickel nitrate and 0.073 g of ferric nitrate were dissolved in 100 mL double distilled water. 4.66 g citric acid was added as a gelling agent with continuous shaking. The pH is maintained at 7 by adding NH_3 solution drop wise. The mixture was allowed to stir for 3 h. When a homogeneous gel starts forming, the mixture was dried at 80 °C to form a gel. The powder obtained was grinded and sintered at 600 °C for 2 h.

2.3. Synthesis of FNZP/PAM nanocomposite

A fine suspension of 500 mg of $\text{Fe}_{0.01}\text{Ni}_{0.01}\text{Zn}_{0.98}\text{O}$ nanoparticles was prepared in 50 mL of distilled water. To this suspension 30 mL of 0.5 M acrylamide solution, 5% ammonium persulphate (APS) and 7% *N,N'*-methylenebisacrylamide (crosslinker) solution was added drop wise. The reaction mixture was constantly stirred at 65 °C for 2 h. The composite gel was washed several times with distilled water. The solution was then centrifuged to remove soluble impurities and by products. The composite was then dried at 50 °C for 5 h in vacuum oven.

2.4. Characterization

The Phase purity and crystalline size of FNZPs and FNZP/PAM nanocomposite were determined by an XPERT-PRO X-ray diffractometer using Cu K α radiation. The morphology of samples was studied using a scanning electron microscope (SEM) QUANTA250 FEI D9393. Elemental analysis was done by EDX equipped with SEM. TEM analysis was performed by high resolution transmission electron microscopy (HRTEM) and small area electron diffraction (SAED) using FEI Tecnai F20 transmission electron microscope. FTIR spectra were recorded by using a Nicolet 5700 FTIR spectrophotometer with the KBr pellet method. The ultraviolet-visible spectra (UV-vis) were recorded using Systronics 2202 double beam spectrophotometer.

2.5. Optical and band gap studies

5 mg of FNZP was dispersed in ethanol. The suspension was then ultrasonicated for 1 h. The UV-vis spectrum was then recorded using double beam spectrophotometer. The same process is repeated for PAM and FNZP/PAM.

2.6. Dye removal

The photocatalytic efficiency of synthesized samples was analyzed by studying the degradation of MG and MB solution in dark as well as sunlight in a slurry type batch reactor [36]. In a typical experiment, the slurry consisting of dye and catalyst suspension was stirred magnetically. For this 0.25 mg/ml photocatalyst (FNZP/PAM) was added to aqueous solution of dye (10^{-5} M).

The double walled pyrex glass vessel containing the slurry was surrounded by thermostatic water circulation arrangement to keep temperature in the range of $30 \pm 0.5^\circ\text{C}$. The pH of mixture was maintained at 7 using acid or base. In the first reaction condition, before exposing the solutions to sunlight, they were kept in dark for 1 h to establish adsorption–desorption equilibrium. The system was then exposed to sunlight. After intervals of time aliquot of 3 ml was taken out and centrifuged to remove catalyst form suspension. The absorption of dye was then recorded using double beam spectrophotometer at 620 nm (MG) and 662 nm (MB). The experiments were performed in month of March with average intensity of sunlight as $29 \times 10^3 \pm 1001\text{x}$. All experiments were performed three times and average values were reported.

In the second reaction condition the coupled effect of adsorption and photocatalysis was also studied on exposing the dye solution containing FNZP/PAM to sunlight without keeping it in dark.

2.7. Antibacterial activity

The antibacterial activity of various synthesized samples was studied against *S. aureus*. The strains of *S. aureus* (MTCC 737) were obtained from IMTech Chandigarh, India. The muller hinton broth (analytical grade) was procured from Him Media, India. The antibacterial activity of FNZP/PAM against *S. aureus* was determined based on batch cultures containing solutions of different concentrations of FNZP/PAM (60, 80, 120, and 160 $\mu\text{g}/\text{mL}$ prepared in distilled water). Sterile conical flasks containing 200 mL nutrient broth medium were sonicated for 10 min after adding the samples to prevent aggregation of the nanoparticles. The flasks were then inoculated with 1 mL of the freshly prepared bacterial suspension (colony forming units 10^8) as per Mcfarlands standards [37]. The flasks were then incubated in an incubator shaker at 200 rpm and 37°C . The bacterial growth was measured using growth curve method by measuring increase in optical density (OD) at 600 nm with a UV spectrophotometer. A positive control (containing FNZP/PAM and nutrient medium, without inoculum) was also kept.

3. Results and discussion

3.1. Characterization

3.1.1. FTIR analysis

The FTIR spectra of FNZP, PAM and FNZP/PAM are shown in Fig. 1. A strong absorption band at 498.0 cm^{-1} is observed in FTIR spectrum of FNZP which is due to Zn–O stretching frequency [38]. The peak at 701 cm^{-1} corresponds to Fe–O stretching [39]. In the FTIR spectrum of PAM the absorption peaks at 3416 cm^{-1} and 3190 cm^{-1} corresponds to O–H stretching and N–H stretching [40] respectively. The characteristic peaks at 1451 cm^{-1} corresponding to C–N stretching [41] 1664 cm^{-1} corresponding to C=O stretching [42] and 2930 cm^{-1} to CH₂ stretching.

The FTIR spectrum of FNZP/PAM indicates that the characteristic peaks of PAM are shifted slightly which was due to bond formation between FNZP and the polymer. The peak corresponding to O–H and N–H stretching was shifted to 3408 cm^{-1} and 3178 cm^{-1} in the nanocomposite. This shift in the absorption confirms the bonding of oxygen of metal oxide to NH group in nanocomposite. The peaks at 2928 cm^{-1} , 1661 cm^{-1} , 1451 cm^{-1} , 3178 cm^{-1} and 467 cm^{-1} correspond to –CH₂ stretching, C=O stretching, C–N stretching, N–H stretching, Zn–O stretching respectively. This also confirms the bonding of FNZP to the polymer matrix.

3.1.2. XRD analysis

Fig. 2 shows the XRD pattern of the FNZP and FNZP/PAM. The diffractogram reveals that, there has been no change in the wurtzite

Table 1
d spacings for $\text{Fe}_{0.01}\text{Ni}_{0.01}\text{Zn}_{0.98}\text{O}$ nanoparticles.

S. No.	Diffracton plane for $\text{Fe}_{0.01}\text{Ni}_{0.01}\text{Zn}_{0.98}\text{O}$ nanoparticles	<i>d</i> spacing (Å)
1	100	2.814
2	002	2.603
3	101	2.476
4	102	1.906
5	110	1.621
6	103	1.477
7	200	1.404
8	112	1.377
9	201	1.370

structure of ZnO after Ni/Fe doping. The XRD pattern for FNZP show broad peaks at the positions of 31.5662, 34.4421, 36.2844, 47.6271, 56.6759, 62.7747, 66.2949, 67.7269, and 69.1416 which were in good agreement with the standard JCPDS file No. 30-1451 for ZnO [43]. The structure can be indexed as the hexagonal wurtzite having space group P63mc [44]. The average crystallite size for FNZP is and 23 nm and for FNZP/PAM is 55 nm. The *d* spacings are calculated using Bragg's diffraction law

$$n\lambda = 2d \sin \theta \quad (1)$$

The calculated *d* spacings for various planes are reported in Table 1. The *d*-spacings and lattice constants for Fe/Ni co doped ZnO show a slight decrease as compared to bare ZnO (JCPDS file No. 30-1451). It implies that the doping most probably occurs by substituting zinc atom in crystal structure, otherwise the lattice parameters would deviate more from the values for undoped ZnO. Thus we can say that no other impurity phase as metallic Ni or Fe and oxide as nickel oxide and iron oxide is found. So doping is successful. The crystallite size is determined using Scherrer's formula

$$p = \frac{K\lambda}{\beta \cos \theta} \quad (2)$$

where *p* is the crystallite size, β is the full width at half maximum, $K = 0.9$ and $\lambda = 1.54\text{ \AA}$ for Cu K α radiation.

The lattice constants for FNZPs as calculated from XRD data have been calculated as $a = b = 3.2492\text{ \AA}$ and $c = 5.2357\text{ \AA}$. The XRD pattern of FNZP/PAM shows that the sample is semi-crystalline and there is a slight decrease in 2 theta values for various planes of FNZP and intensity also.

3.1.3. SEM and EDX analysis

Fig. 3a and b illustrates the SEM images of FNZP and FNZP/PAM respectively. The SEM micrograph shows that FNZPs are spherical in shape with a little agglomeration. There has also some porosity observed which may be due to sintering process. The SEM micrograph of FNZP/PAM shows the formation of a hybrid nanocomposite. The PAM exhibits irregular sheet like morphology. The FNZP granules are uniformly distributed over the matrix.

The EDX pattern of FNZP (Fig. 3c) shows the presence of Fe, Ni, Zn and O in the sample. The stoichiometry in the final product is nearly the same as in starting. The EDX pattern of FNZP/PAM (Fig. 3d) shows the clear presence of Fe, Ni, Zn, C, N and O in the sample.

3.1.4. TEM analysis

The HRTEM image of FNZP (Fig. 4a) shows that particles have mixed shapes as spherical and hexagonal. The fringes are clearly visible. The SAED pattern (Fig. 4b) reveals the sample is highly crystalline. The Low resolution TEM image of FNZP/PAM (Fig. 4c) shows that polyacrylamide is in a gel form and FNZPs are dispersed in polymer matrix. The FNZP nanoparticles are visible on higher resolutions because of dominance of the polymer matrix. Fig. 4(d) shows the SAED pattern of FNZP/PAM nanocomposite. From SAED

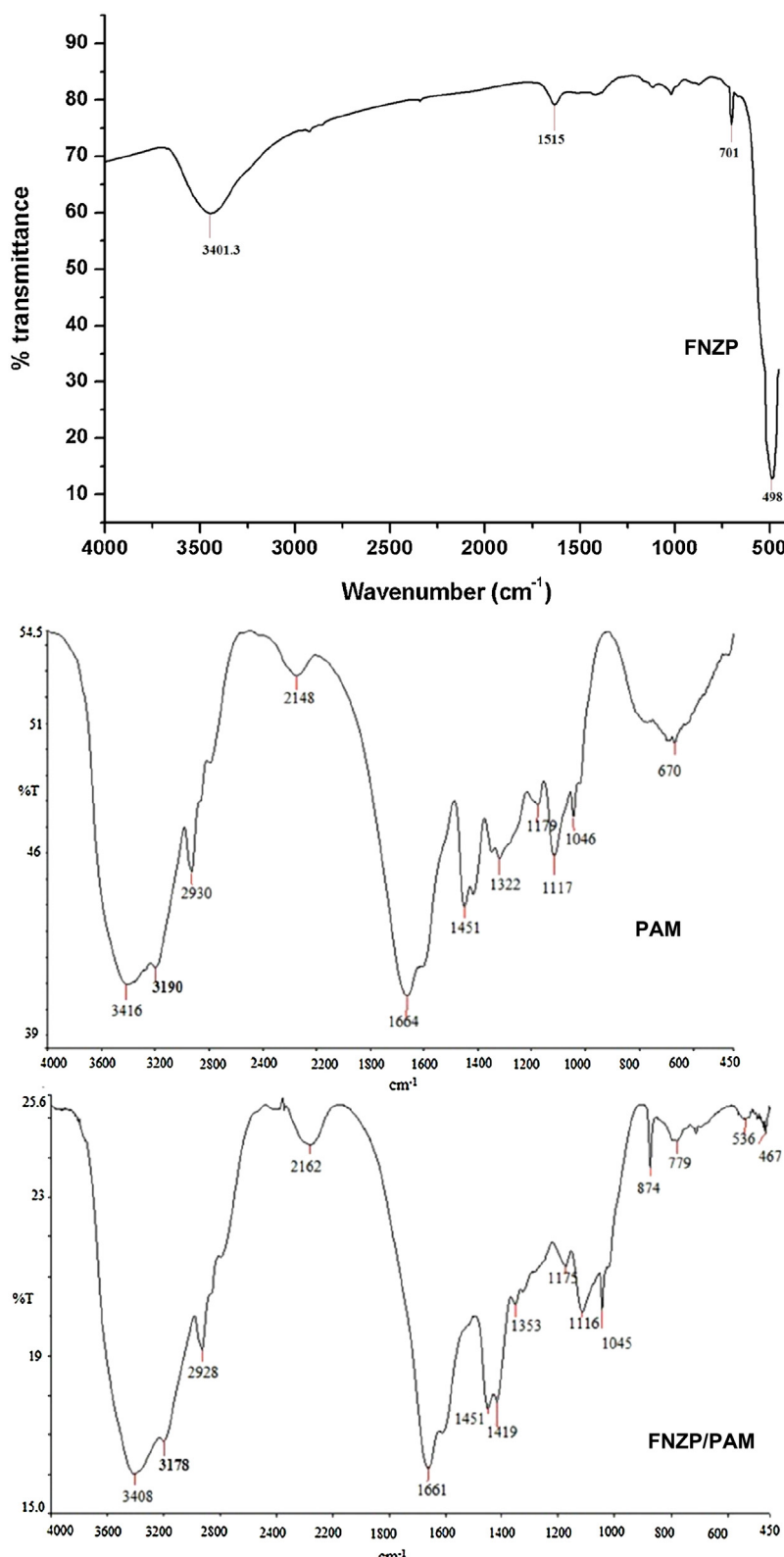


Fig. 1. FTIR spectra of FNZP, PAM and FNZP/PAM.

pattern it has been inferred that FNZP is present in crystalline form but the crystallinity is low because of interaction with the polymer matrix. These results were also supported by XRD results. The average particle size for FNZP is 15–30 nm and for FNZP/PAM is 35–60 nm.

3.1.5. UV-vis analysis

The UV-vis absorption spectrum of the FNZP (Fig. 5b) shows absorption peak around 385 nm which is the characteristic single peak of hexagonal ZnO nanoparticles. But there has been a shift in the absorption towards the longer wavelength because of doping by

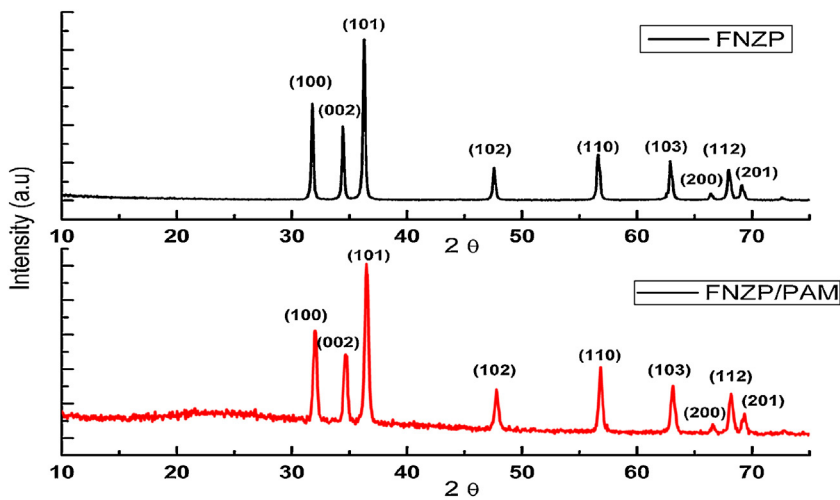


Fig. 2. XRD pattern of FNZP and FNZP/PAM.

transition metal ions (bare ZnO absorb at 378 nm). The red shift was common in transition metal doped Zinc oxide [45]. A higher visible absorption can be observed in case of FNZP/PAM (Fig. 5a). The band gaps of nanoparticles and composite were calculated using Tauc Relation [46]

$$\alpha h\nu = B(h\nu - E_g)^n \quad (3)$$

where α = absorption coefficient = 2.303 A/l [47], E_g = optical band gap, B = band tailing parameter, $h\nu$ is the photon energy, and $n = 1/2$ for direct band gap. The optical band gap is determined by extrapolating the straight portion of curve between $(\alpha h\nu)^2$ and $h\nu$ when

$\alpha = 0$. The band gap as calculated from Tauc plot is 3.17 eV for FNZP (Fig. 5c) and 3.07 eV for FNZP/PAM.

3.2. Dye removal

The photocatalytic degradation of MG and MB in presence of FNZP and FNZP/PAM as catalysts was investigated under sunlight irradiation. The system was exposed to two reaction conditions: equilibrium adsorption followed by photocatalysis and coupled adsorption and photocatalysis.

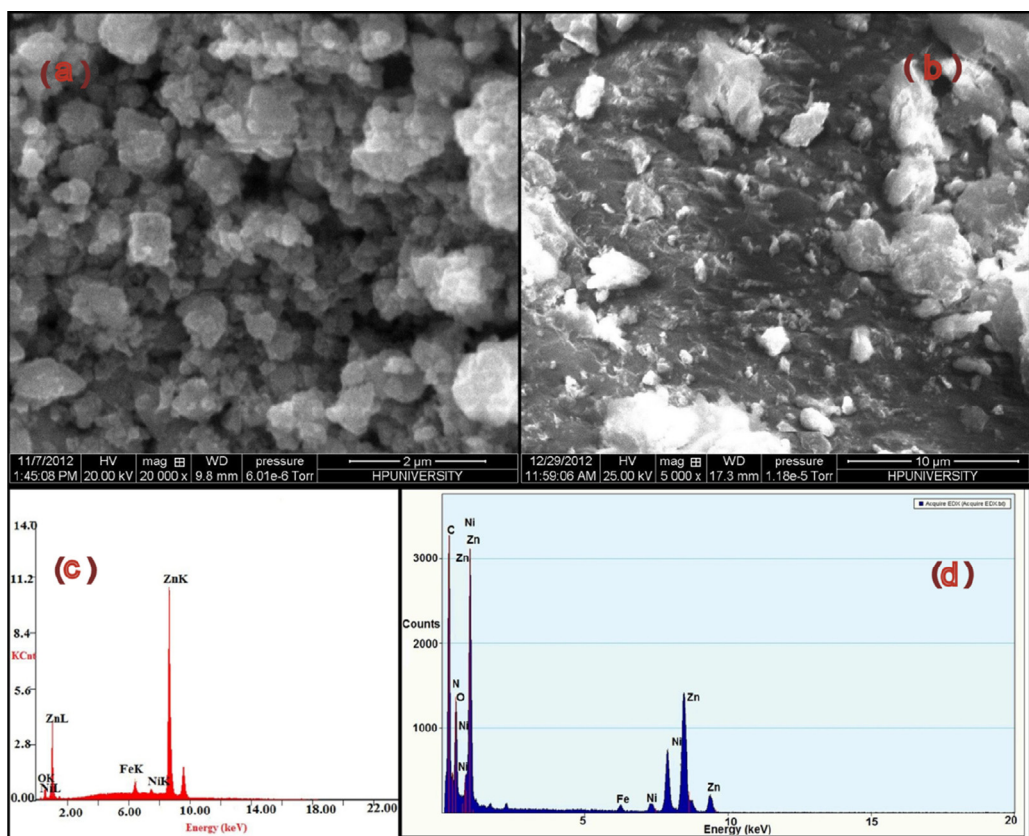


Fig. 3. (a) SEM micrograph of FNZP, (b) SEM micrograph of FNZP/PAM, (c) EDX pattern of FNZP and (d) EDX pattern of FNZP/PAM.

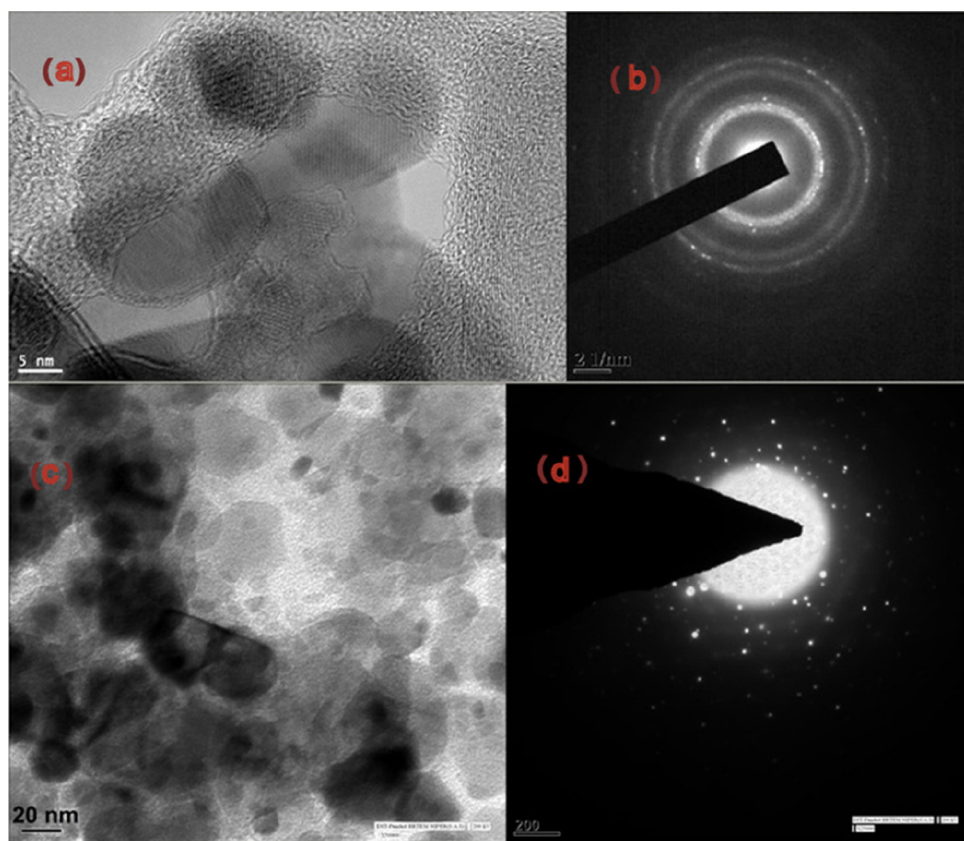


Fig. 4. (a) HRTEM image of FNZP, (b) SAED pattern of FNZP, (c) TEM image of FNZP/PAM and (d) SAED pattern of FNZP/PAM.

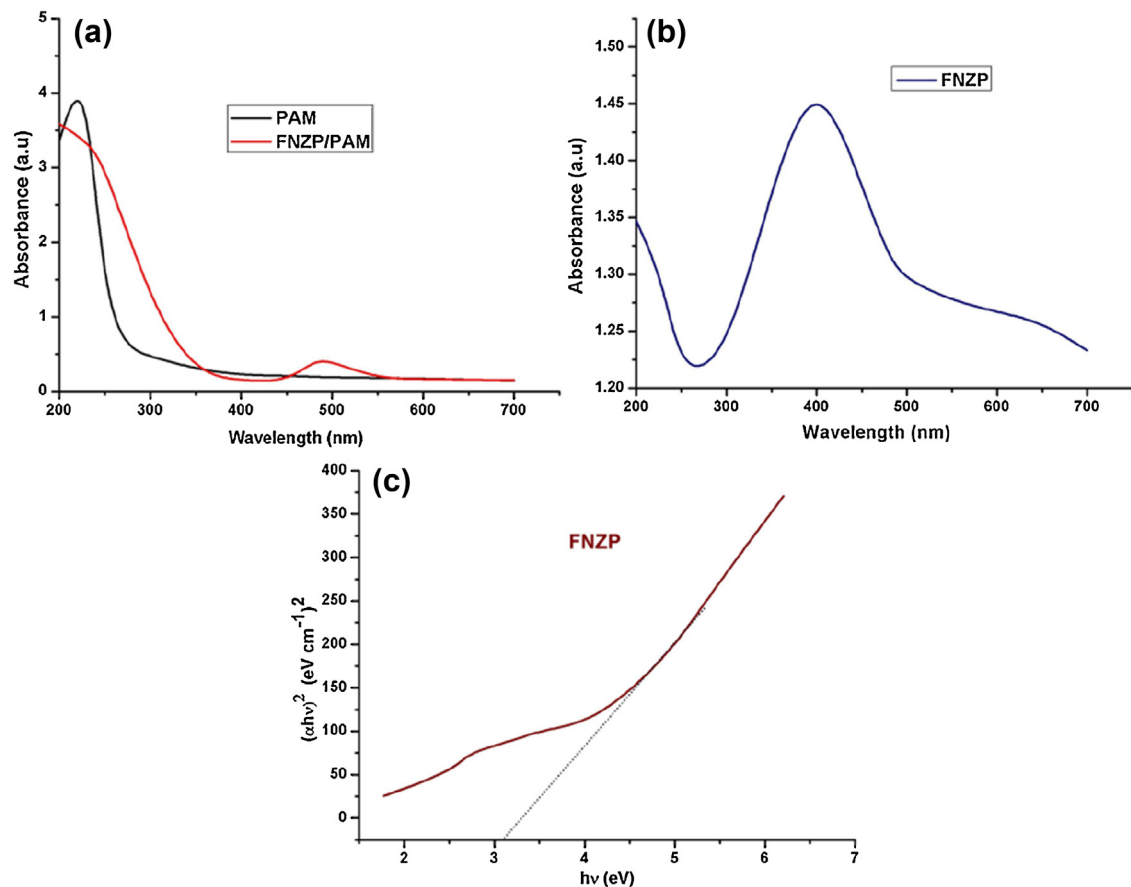


Fig. 5. (a) UV–vis spectra of PAM and FNZP/PAM, (b) UV–vis spectrum of FNZP and (c) Tauc Plot for FNZP.

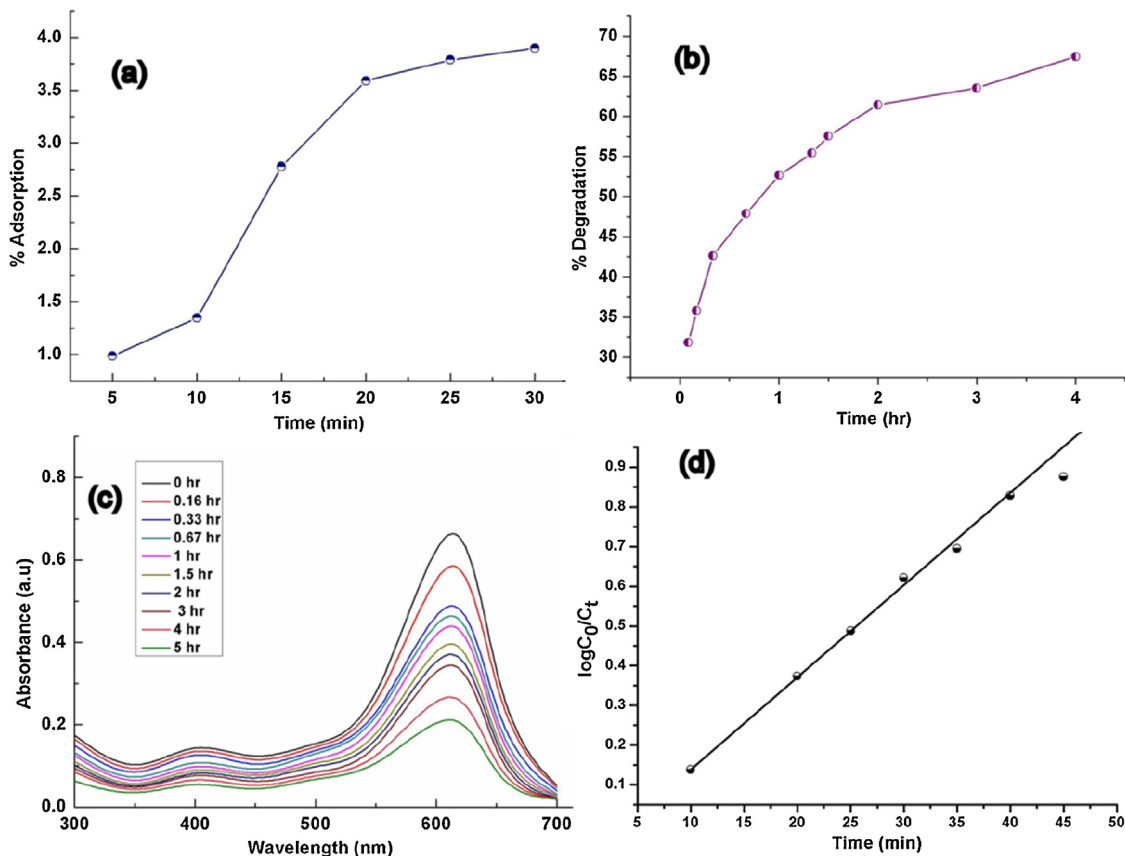


Fig. 6. (a) Adsorption of MG onto FNZP in dark, (b) photodegradation of MG in presence of FNZP on illumination, (c) spectrum of MG dye in presence of FNZP and (d) pseudo first order kinetics for photodegradation of MG in presence of FNZP (Initial concentration of MG 10^{-5} M, pH = 7, temperature = 30 ± 0.5 °C).

3.2.1. Equilibrium adsorption followed by photocatalysis

The first reaction condition is keeping the dye solution containing FNZP and FNZP/PAM in dark to establish adsorption–desorption equilibrium. After that the suspensions were exposed to natural sunlight for further photodegradation. Fig. 6(a) and (b) depict the removal of MG (10^{-5} M) by FNZP suspension in dark and sunlight respectively. It has been observed that only 3.89% of dye is adsorbed by FNZP. Followed by photodegradation of dye in sunlight 78.47% degradation in 5 h was achieved. Thus FNZP is a better photocatalytic agent than an adsorbent. However a 5.17% adsorption (Fig. 8a) and 80.31% photodegradation (Fig. 8b) was achieved in case of MB (10^{-5} M). Better results were obtained for initial dye concentration of 10^{-6} M.

The % degradation of dye is calculated using following formula

$$\% \text{ degradation} = \frac{C_0 - C_t}{C_0} \times 100 \quad (4)$$

where C_0 = initial concentration of dye before illumination and C_t after time t .

When FNZPs were irradiated with UV-vis light electron–hole pairs are generated, which react with water to produce hydroxyl and super-oxide radicals which disrupt the conjugation in organic molecules such as dye and may also mineralize them. The band gap of ZnO is 3.37 eV, which can be overcome by absorbing UV and visible light [48]. But photocatalytic activity has been observed less in sunlight (contains only 3–5% UV). The absorption was increased on doping. The effect of transition metal ions dopants on the photocatalytic activity was the dynamics of electron–hole recombination and interfacial charge transfer. The Ni^{2+} and Fe^{3+} ions act as electron traps which form unstable ions and which combine with oxygen and hydroxyl ions to form hydroxyl and superoxide ion radicals.

The results obtained for Fe/Ni co doped ZnO nanoparticles in visible light are far better than earlier reported ones for Ni (dopant percentage 2%, 5%, 10%) [32] and Fe (dopant percentage 2–5%) doped ZnO [49].

Table 2 shows the various parameters calculated for degradation of MG and MB in presence of FNZP and FNZP/PAM under both the reaction conditions. In case of FNZP/PAM we achieved a 27.45% adsorption of MG (Fig. 7a) and 31.44% of MB (Fig. 9a) in 1 h when the suspensions were kept in dark.

The crosslinked polyacrylamide gel possesses excellent adsorbing properties [33,50]. The photodegradation process depends on concentration of dye in bulk solution and on photocatalyst surfaces [51,52]. The adsorption onto FNZP/PAM is important for the study of photodegradation activity of the composite. The total dye concentration at any time is

$$C = C_b + C_s \quad (5)$$

where C_b and C_s are the concentrations of dye in bulk and on the surface respectively. The concentration of dye adsorbed onto catalyst surface is calculated as [24]

$$C_s = (C_0 - C_e) \frac{V}{M} \quad (6)$$

where V is the volume of solution and M is the mass of adsorbent.

As indicated by Figs. 7(b) and 9(b), totally 92.13% of MG and 95.78% of MB (initial concentration 10^{-5} M) was photodegraded in presence of FNZP/PAM in 4 h. Similar higher efficiency was achieved for lower dye concentration (10^{-6} M).

Several reports claim that the rate of photodegradation of various dyes fitted a pseudo first order kinetic model [53]:

$$\ln(C_0/C_t) = k_{\text{app}} t \quad (7)$$

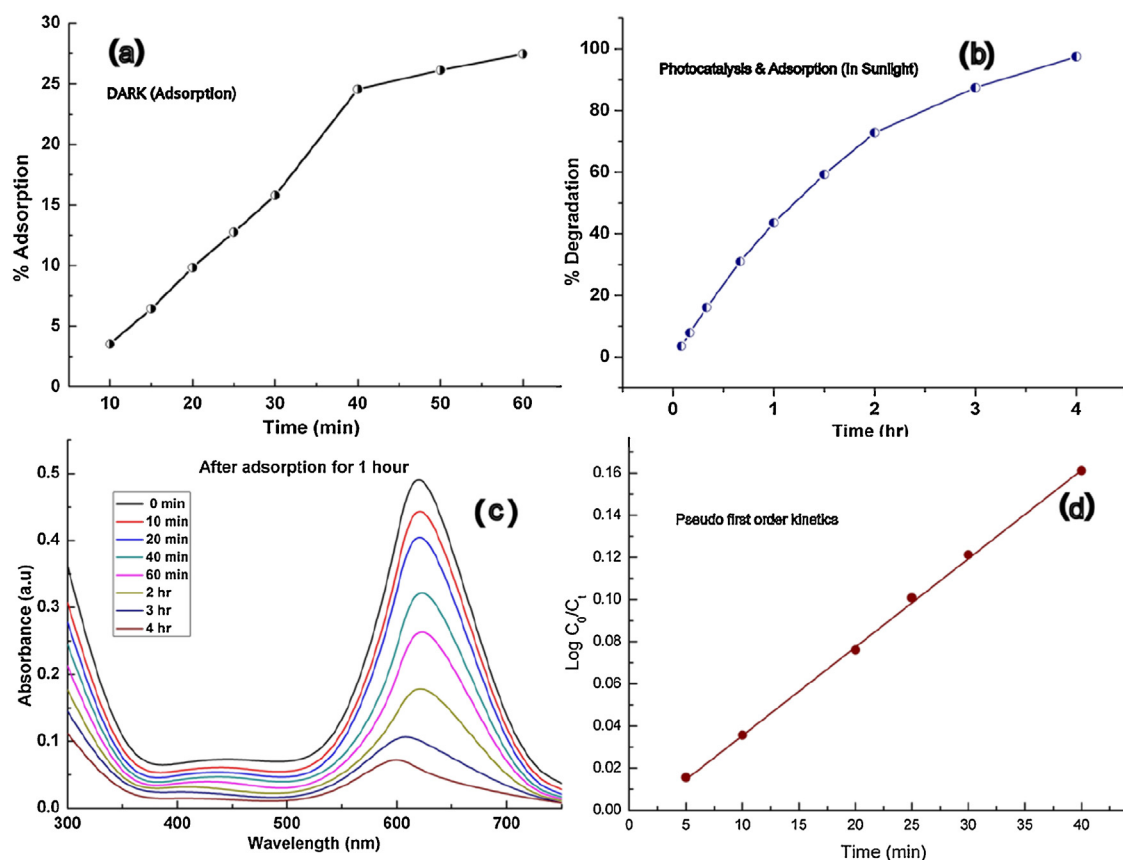


Fig. 7. (a) Adsorption of MG onto FNZP/PAM in dark, (b) photodegradation of MG in presence of FNZP/PAM on illumination, (c) spectrum of MG in presence of FNZP/PAM (Initial concentration of MG 10^{-5} M, pH = 7, temperature = $30 \pm 0.5^\circ\text{C}$).

where k_{app} is the apparent rate constant, C_0 is the concentrations of dye before illumination and C_t the concentration of dyes at time t . Table 3 represents the apparent and overall rate constants and linear regression coefficients for photodegradation of MB and MG under both reaction conditions. The graph between $\log C_0/C_t$ vs t for photodegradation of MG (Fig. 7d) and MB (Fig. 9d) in presence of FNZP/PAM shows that process follows pseudo first order kinetics. Table 3 shows rate constants and linear regression coefficients for both the reaction conditions. The rate constants for MG and MB removal are 0.018 min^{-1} and 0.027 min^{-1} respectively and for FNZP/PAM are 0.026 min^{-1} and 0.028 min^{-1} . The results were better for 10^{-6} M dye concentration. The results infer that FNZP/PAM is better agent than FNZP for removal of MB and MG by adsorption followed by photocatalysis.

3.2.2. Coupled adsorption and photocatalysis

To study the effect of adsorption onto the degradation activity of FNZP and FNZP/PAM the suspensions containing the photocatalysts and dyes MB and MG were subjected to other reaction condition i.e. coupled adsorption and photocatalysis. Fig. 10(a) and

(b) shows the extent of degradation of MG and MB during coupled process in presence of FNZP/PAM respectively. A whopping 96.13% removal of MG and 97.56% removal of MB respectively were achieved in 2 hours of illumination for initial dye concentration of 10^{-5} M. However higher removal was achieved for initial concentration of 10^{-6} M. The overall process of dye degradation follows a pseudo first order kinetics with overall rate constant (k_0) 0.048 min^{-1} and 0.051 min^{-1} for MG (Fig. 10c) and MB (Fig. 10d) removal respectively. The rate constants clearly reveal a higher rate of photodegradation than previous reaction condition.

The coupled adsorption and photocatalysis of dyes onto FNZP/PAM involves simultaneous adsorption of dye onto photocatalyst and generation of electron hole pair from FNZP on absorption of visible light. The photoexcitation of organic dye plays an important role in degradation. The electron transfer leads to formation of adsorbed dye radical cation which further produces oxygen radical anion which brings about degradation of organic dye by disruption of conjugation. Generally it is believed that photocatalytic efficiency can be enhanced by adsorption of adsorbate onto the

Table 2

Removal of MG and MB by FNZP and FNZP/PAM under two reaction conditions: equilibrium adsorption followed by catalysis and coupled adsorption and photocatalysis.

		Fe _{0.01} Ni _{0.01} Zn _{0.98} O		Fe _{0.01} Ni _{0.01} Zn _{0.98} O/PAM		
		Dark	Sunlight	Dark	Sunlight	Coupled adsorption + photocatalysis % age removal (in 2 h)
		% adsorption (in 1 h)	% degradation (in 5 h)	% adsorption (in 1 h)	% degradation (in 4 h)	
MG	10^{-5} M	3.89	78.47	27.45	92.13	96.13
	10^{-6} M	4.02	82.14	28.33	93.77	97.45
MB	10^{-5} M	5.17	80.31	31.44	95.78	97.56
	10^{-6} M	5.21	80.44	30.45	96.31	97.67

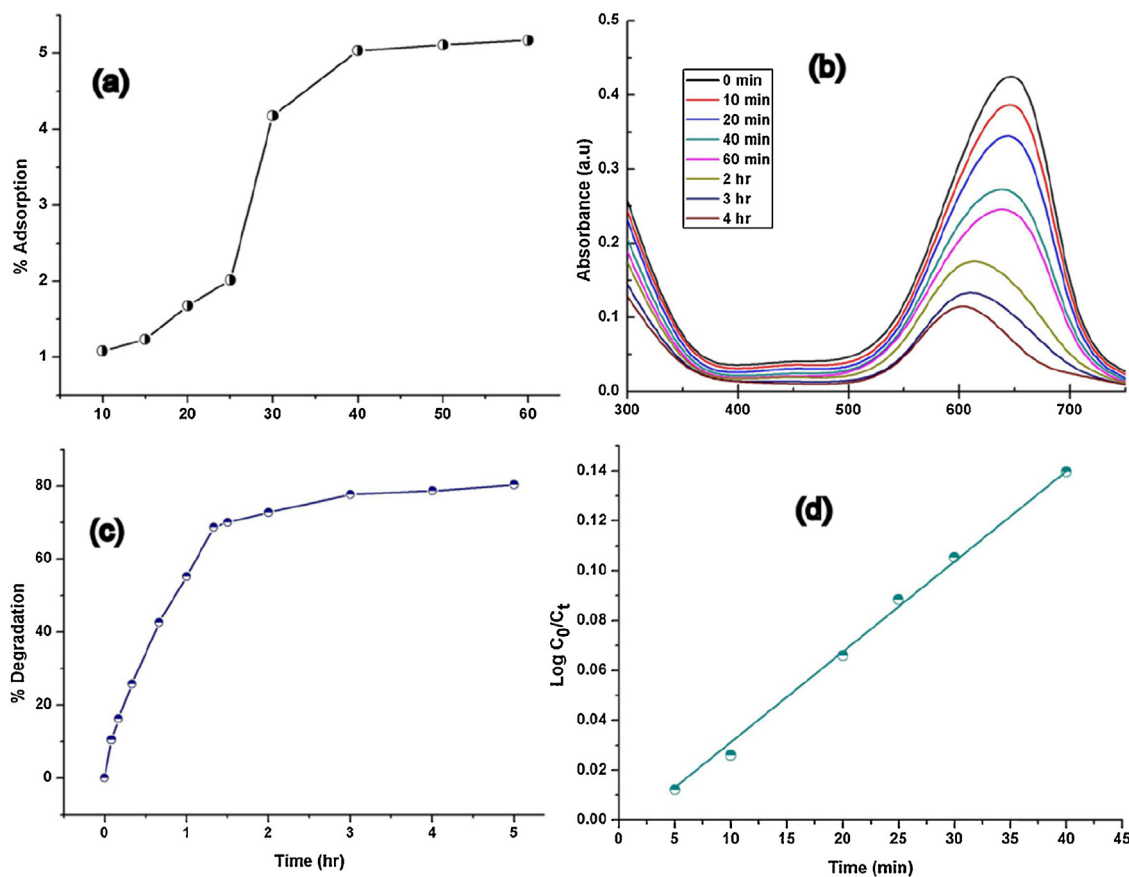
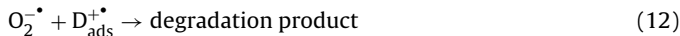
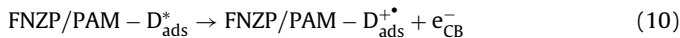
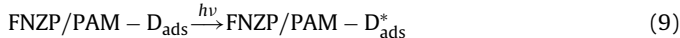
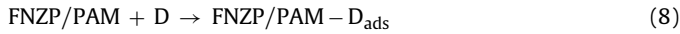


Fig. 8. (a) Adsorption of MB onto FNZP in dark, (b) photodegradation of MB in presence of FNZP on illumination, (c) spectrum of MB in presence of FNZP and (d) pseudo first order kinetics for photodegradation of MB in presence of FNZP (initial concentration of MB 10^{-5} M, pH = 7, temperature = 30 ± 0.5 °C).

catalyst [54]. The dye removal mechanism under coupled adsorption and photocatalysis can be represented by Eqs. (8)–(12)



Alternatively it was suggested that as soon as dye is adsorbed onto FNZP/PAM and system is exposed to sunlight, there is a simultaneous production of electron–hole pair in FNZP. This brings about the degradation of adsorbed dye faster as for the dye present in the bulk solution. There is a generation of OH[·] free radical leading to

disruption of conjugation [55]. The pH of the solution was maintained as 7. In a basic condition, the negatively charged phenolic hydroxyl groups become potentially active sites (NH₂) and could be attracted by the ammonium groups in the absorbents [50]. At basic pH there was no protonation of NH₂ groups, so they can easily bind to cationic dyes as MB and MG. Based on the characterization results and dye removal experiments, a mechanism for the adsorption and photocatalytic removal of cationic dye by FNZP/PAM is anticipated and described in Fig. 11. FNZP/PAM presents an adequate morphology for cationic dye adsorption. It appears that adsorption of MB dye is caused by the fact that COO[−], CONH₂, OH[−] functionalities of cross linked PAM (mildly basic medium) favours the electrostatic interactions with cationic dye.

Both the schemes and the results suggest that coupled adsorption and photocatalysis is a better reaction condition for dye removal. In the first reaction condition (equilibrium adsorption followed by photocatalysis) there is possibility that the surface of photocatalyst is covered by dye molecules and so degradation of MB and MG is suppressed. However in case of second reaction condition

Table 3

Apparent rate constants and linear regression coefficients from $\log C_0/C_t$ vs T plots for different dye concentrations.

	Fe _{0.01} Ni _{0.01} Zn _{0.98} O		Fe _{0.01} Ni _{0.01} Zn _{0.98} O/PAM			
	Photocatalysis		Photocatalysis		Coupled adsorption + photocatalysis	
	k_{app} (min^{-1})	R^2	k_{app} (min^{-1})	R^2	k_0 (min^{-1})	
MG	10 ⁻⁵ M	0.018	0.98	0.026	0.99	0.048
	10 ⁻⁶ M	0.022	0.99	0.031	0.98	0.052
MB	10 ⁻⁵ M	0.027	0.99	0.028	0.99	0.051
	10 ⁻⁶ M	0.042	0.99	0.034	0.99	0.054

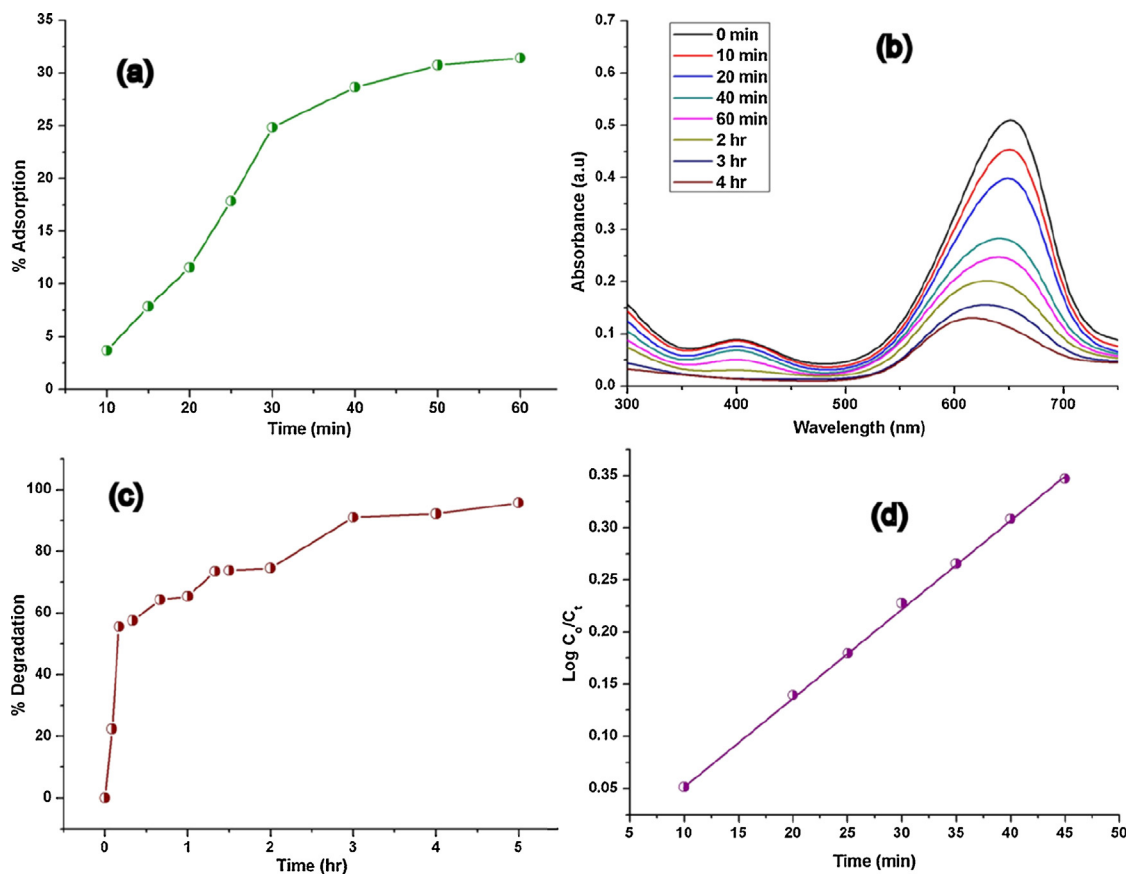


Fig. 9. (a) Adsorption of MB onto FNZP/PAM in dark, (b) photodegradation of MB in presence of FNZP/PAM on illumination, (c) spectrum of MB in presence of FNZP/PAM and (d) pseudo first order kinetics for photodegradation of MB in presence of FNZP/PAM (initial concentration of MB 10^{-5} M, pH = 7, temperature = 30 ± 0.5 °C).

(coupled adsorption and photocatalysis) we achieve higher and faster removal of both the dyes because as soon as dye is adsorbed onto FNZP/PAM, it is degraded by generated free radicals.

To evaluate the photodegradation reusability of FNZP/PAM, it was reused for several photocatalytic experiments for illumination of 6 h and 6 cycles. Fig. 12 shows the recycling efficiency of the FNZP/PAM. Under several usages the sample can be used for photodegradation of dye. After 6 h of illumination we achieve almost complete dye removal for the first usage, but for the sixth usage 75.11% efficiency is achieved. The retardation of photocatalytic activity is due to accumulation of intermediates on the surface leading to fall in concentration of OH[•] [56]. The filtration of FNZP/PAM was quick and easy due to gel formation ability of crosslinked polyacrylamide. FNZP/PAM was easily recycled with 75.11% efficiency (in sixth cycle) confirming the reusability of nanocomposite in photodegradation process. The composite is easy to synthesize, inexpensive and recoverable.

The obtained results were compared with various photocatalytic systems (Table 4). FNZP/PAM nanocomposite was highly efficient under solar radiation as compared to reported photocatalytic processes under UV irradiation. It was observed that low dopant concentration is useful in UV region. However, we have achieved significant degradation of methylene blue and malachite green under sunlight at very low dopant concentrations. The dye removal efficiency was further increased in case of FNZP/PAM. For FNZP/PAM the degradation time is only 120 min under coupled adsorption and photocatalysis. FNZP/PAM displayed significant dye removal in both the investigated reaction conditions (equilibrium adsorption followed by photocatalysis and coupled process) under natural sunlight. PAM is popularly used as a flocculant and FNZP. The exceptionally good photocatalytic behaviour of the

inexpensive composite enhances its properties for waste water treatment.

3.3. Thermal stability

Fig. 13 represents the thermograms of polyacrylamide (PAM), FNZP and FNZP/PAM. The TGA curve of FNZP shows insignificant weight loss. The slight weight loss around 200 °C may be due to loss of chemisorbed water molecules [65]. PAM showed four steps of weight loss [66]. The weight loss at 80 °C was attributable to loss of moisture, while those coincided with the weak drop of the TGA curve at 200 °C can be related to thermal processes involving both melting of the PAM chains and onset of degradation. In PAM polymer, the second step of weight loss started at about 200 °C and attained 15% and 27.5% at 300 and 350 °C, respectively.

The first stage decomposition may be attributed to the thermo-oxidative cleavage of the weak and unstable linkages, i.e. methylene groups, leading to thermal degradation of PAM producing low molecular weight gases such as H₂O, CO₂, NH₃, resulting also from the breakdown of side chain groups of amino acid residues. The drop at above 300 °C was indicative of the occurrence of more extensive thermal degradation processes and being due to the cleavage of the imides linkages. At 500 °C there is a weight loss of 35.7%. There was a weight loss from 500 °C onwards; this is attributed to the oxidation of residual carbon.

We observe from TGA curve of FNZP/PAM nanocomposite that the thermal stability of polyacrylamide is enhanced on incorporation of FNZP nanoparticles into its matrix. It is visible in the thermogram that the weight loss at 350 °C in composite is not so sharp as in PAM. A total 19.86% weight loss is reported. Thus FNZP/PAM is thermally more stable than PAM.

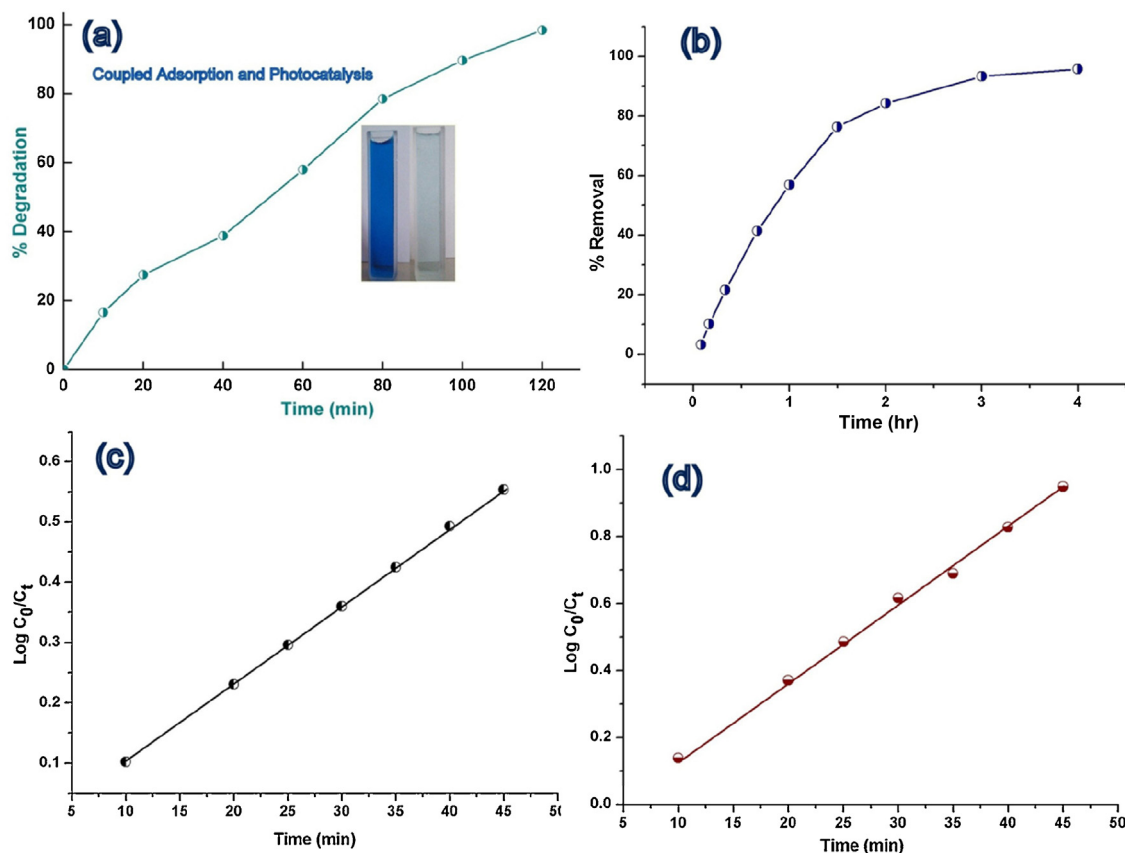


Fig. 10. (a) Extent of removal of MG by coupled adsorption and photocatalysis in presence of FNZP/PAM, (b) extent of removal of MB by coupled adsorption and photocatalysis, (c) kinetics for removal of MG by coupled process and (d) kinetics for removal of MB by coupled process (initial concentration of dyes 10^{-5} M, pH = 7, temperature = $30 \pm 0.5^\circ\text{C}$).

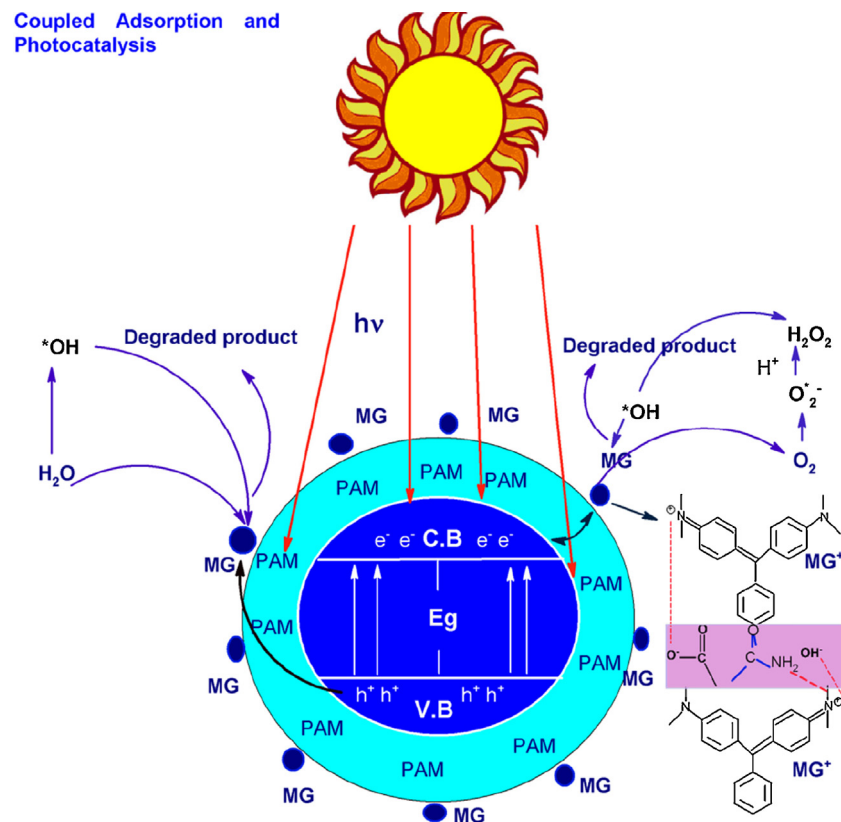


Fig. 11. Suggested mechanism of MG removal by FNZP/PAM under coupled process.

Table 4

Different photocatalytic systems for dye removal from aqueous phase.

Photocatalyst	Irradiation source	Dye	Decolourisation time (min)	Reference
ZnO	UV	Methylene orange Dichlorobenzene	180 90	[30]
Degusa P-25	UV	Methylene blue	90	[30]
Ni (0.2%) doped ZnO	UV	Rhodamine B	210	[58]
Mn (0.3%) doped TiO ₂	UV	Methylene blue	60	[60]
Co (0.3%) doped TiO ₂	UV	Methylene blue	60	[60]
Zn (5%) doped TiO ₂	UV	Methylene blue	300	[61]
Fe (0.7%) doped ZnO	UV	Methylene orange Dichlorobenzene	120 60	[30]
V ⁵⁺ (0.1%) doped TiO ₂	Solar light	Congo red	180	[57]
Ag ⁺ (0.95%) doped TiO ₂	UV	Crystal violet Methyl red	90	[62]
Ni ²⁺ doped (5%) ZnO	UV	Rhodamine B	90	[32]
TiO ₂ /PANI	Solar light	Methylene blue	300	[63]
PANI/ZnO	Solar light	Methylene blue	240	[64]
FNZP/PAM	Solar light	Malachite green Malachite green Methylene blue	240 120 120	Present study

3.4. Antibacterial study

The antibacterial activity of synthesized nanomaterials was also tested against *S. aureus*. Fig. 14 represents growth curve of *S. aureus* in presence of FNZP/PAM. A concentration of 60 µg/ml was not quite effective in bacterial inhibition compared to growth of *S. aureus* in control medium. However at

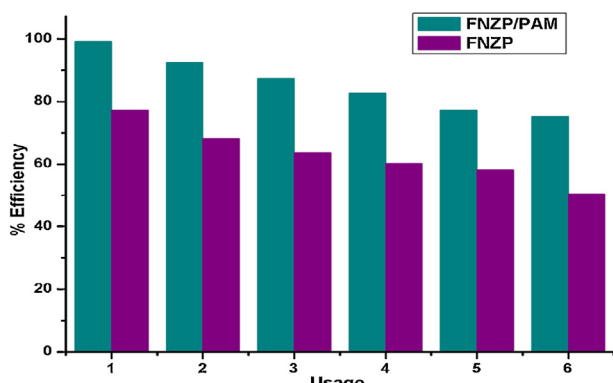


Fig. 12. Efficiency of FNZP/PAM and FNZP for several usages for MG removal (coupled adsorption and photocatalysis).

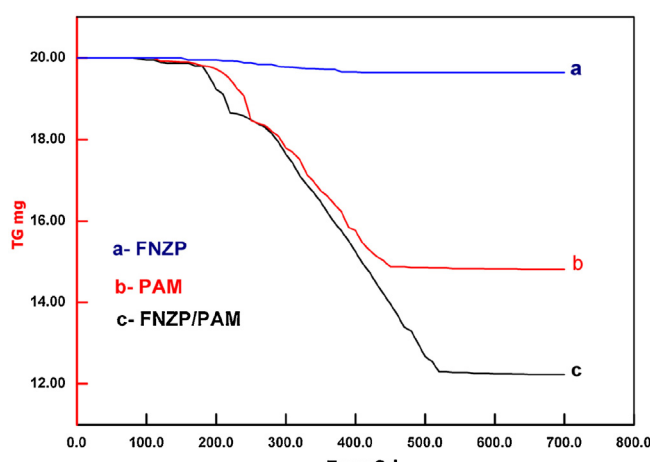


Fig. 13. TGA thermogram for FNZP, PAM and FNZP/PAM.

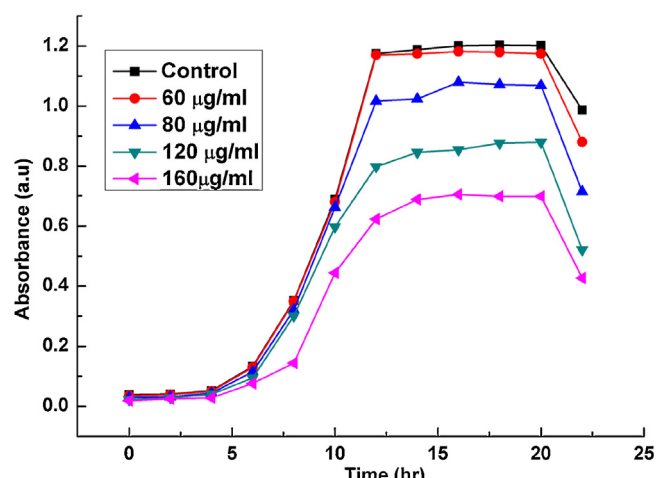


Fig. 14. Growth curve of *S. aureus* in presence of FNZP/PAM.

concentration 80 µg/ml the inhibition is observed after 10 h of incubation. A concentration of 120 µg/ml of FNZP/PAM nanocomposite was effective in inhibiting the growth of *S. aureus* for complete duration of incubation.

The effectiveness of FNZP/PAM on microorganism can be explained on the basis of the reactive oxygen species (OH^- , H_2O_2 and O_2^{2-} , OH^+) released on the surface of FNZP/PAM, which cause fatal damage to microorganisms.

4. Conclusions

The advantageous outcomes obtained by the developed methodology of coupled adsorption and photocatalysis are very promising. Our studies clearly revealed that FNZP/PAM nanocomposite shows better dye removing capability under coupled adsorption and photodegradation. Nevertheless FNZP nanoparticles also exhibited a decent photodegradation activity but scores low due to poor adsorption. Under the coupled condition the lower adsorption and simultaneous photodegradation was responsible for better activity. The ongoing coupled process follows a pseudo first order kinetics as a whole. The simple and ease of synthesis, higher photodegradation activity, good antimicrobial action and reusability of the FNZP/PAM can be used for treatment of waste water.

Acknowledgements

The authors will like to thank Centre for Scientific and Industrial Research (CSIR) and University Grants Commission, Government of India for providing financial aid in form of Junior Research Fellowship. The authors will also acknowledge Mr. Vinod Chaudhary, ICON International for HRTEM support.

References

- [1] G. Crinic, Bioresour. Technol. 97 (2006) 1061–1085.
- [2] A.S. Ozcan, B. Erdem, A. Ozcan, Colloids Surf., A 266 (2005) 73–81.
- [3] R. Sivaraj, C. Namasivayam, K. Kadirvelu, Waste Manage. 21 (2007) 105–170.
- [4] S. Sarmah, A. Kumar, Indian J. Phys. 85 (2011) 713–726.
- [5] T.D. Kose, S.P. Ramteke, Int. J. Composite Mater. 2 (4) (2012) 44–47.
- [6] V. Fischer, I. Lieberwirth, G. Jakob, R. Landfester, R. Munoz-Espi, Adv. Funct. Mater. 23 (4) (2013) 451–466.
- [7] Y.D. Liu, F.F. Fang, H.J. Chai, Y. Sego, Colloids Surf., A 381 (2012) 12–22.
- [8] S.B. Kondawar, S.P. Agrawal, S.H. Nimkar, H.J. Sharma, P.T. Patil, Adv. Mat. Lett. 3 (5) (2012) 393–398.
- [9] T.J. Pinnavaia, Science 220 (1983) 365–371.
- [10] Y. Wang, N. Herron, Science 27 (1996) 632–634.
- [11] J.G. Winiarz, L.M. Zhang, M. Lal, C.S. Friend, P.N. Prasad, J. Am. Chem. Soc. 121 (1999) 5287–5295.
- [12] M. Wang, Y. Lian, X. Wang, Curr. Appl. Phys. 9 (2009) 189–194.
- [13] W. Kangwansupamonkon, W. Jitbunpot, S. Kiatkamjornwong, Polym. Degrad. Stab. 95 (2010) 1894–1902.
- [14] C. Sanchez, B. LeBeau, F. Ribot, J. Sol-Gel Sci. Technol. 19 (2000) 31–38.
- [15] X. Gao, Y. Zhu, Y. Zhao, Z. Wang, D. An, Y. Ma, S. Guan, Y. Du, B. Zhou, Appl. Surf. Sci. 257 (2011) 4719–4724.
- [16] S. Qin, L. Wang, X. Zhang, G. Su, Appl. Surf. Sci. 257 (2010) 731–735.
- [17] Q. Wan, C.L. Lin, X.B. Yu, T.H. Wang, Appl. Phys. Lett. 84 (2004) 184–186.
- [18] S.H. Jo, J.Y. Lao, Z.F. Ren, R.A. Farrer, T. Baldacchini, J.T. Fourkas, Appl. Phys. Lett. 83 (2003) 4821–4823.
- [19] O. Lupon, L. Chow, S. Shishiyaru, E. Monaco, T. Shishiyaru, V. Şontea, B. Roldan Cuena, A. Naitabdi, S. Park, A. Schulte, Mater. Res. Bull. 44 (2009) 63–69.
- [20] H.Q. Yan, R.R. He, J. Johnson, M. Law, R.J. Saykally, P. Yang, J. Am. Chem. Soc. 125 (2003) 4728–4729.
- [21] B.F. Martinson, J.W. Elam, J.T. Hupp, M.J. Pellin, Nano Lett. 7 (2007) 2183–2187.
- [22] Z.L. Wang, J.H. Song, Science 312 (2006) 242–246.
- [23] X. Ren, D. Han, D. Chen, F. Tang, Mater. Res. Bull. 42 (2007) 807–813.
- [24] V.K. Gupta, D. Pathania, S. Agarwal, P. Singh, J. Hazard. Mater. 243 (2012) 179–186.
- [25] B.K. Korbahti, K. Artut, C. Gecgel, A. Ozer, Chem. Eng. J. 173 (2011) 677–688.
- [26] R. Wu, J. Qu, H. He, Y. Yu, Appl. Catal., B 48 (2004) 49–56.
- [27] R. Ullah, J. Dutta, J. Hazard. Mater. 156 (2008) 194–200.
- [28] R. Wang, J.H. Xin, Y. Tang, H. Liu, L. Xu, J. Hu, Appl. Surf. Sci. 227 (2004) 312–317.
- [29] R. He, R.K. Hocky, T. Tsuzuki, Mater. Chem. Phys. 32 (2012) 1035–1040.
- [30] Y. Zhang, M.K. Ram, E.K. Stefanakis, D.Y. Goswami, Surf. Coat. Technol. 217 (2013) 119–123.
- [31] H. Xianghong, H. Xinyou, M. Hongkui, Y. Zhixi, Appl. Mech. Mater. 182–183 (2012) 130–134.
- [32] J. Zhao, L. Wang, X. Yan, Y. Yang, Y. Lei, J. Zhou, Y. Huang, Y. Gu, Y. Zhang, Mater. Res. Bull. 46 (8) (2011) 1207–1210.
- [33] M. Zendehdel, A. Barati, H. Alikhani, A. Hekmat, Iranian J. Environ. Health. Sci. Eng. 7 (5) (2010) 423–428.
- [34] J. Chen, K. Park, J. Control. Release 65 (1–2) (2000) 73–82.
- [35] V.A. Myagchenkov, V.F. Kurenkov, Polym. Plast. Technol. Eng. 30 (2–3) (1991) 109–135.
- [36] V.K. Gupta, S. Agarwal, D. Pathania, N.C. Kothiyal, G. Sharma, Carbohydr. Polym. 96 (2013) 277–283.
- [37] P.R. Murray, E.J. Baron, J.H. Jorgensen, M.L. Landry, M.A. Pfaller, Manual of Clinical Microbiology, 9th ed., ASM Press, Washington, DC, 2007.
- [38] N. Faal Hamedani, F. Farzaneh, J. Sci. Islam. Repub. 17 (3) (2006) 231–234.
- [39] H. Qiao, Z. Wei, H. Yang, L. Zhu, X. Yan, J. Nanomater. 2009 (2009), Article ID 795928, 5 p.
- [40] Q. Tang, J. Wu, H. Sun, J. Lin, S. Fan, D. Hu, Carbohydr. Polym. 74 (2008) 215–219.
- [41] D. Li, X. Zhang, J. Yao, G.P. Simon, H. Wang, Chem. Commun. 47 (2011) 1710–1712.
- [42] R.K. Shamsudeen, S. Nair, V.G. Jayakumari, Ind. J. Eng. Mater. 13 (2006) 62–68.
- [43] W.H. Zhang, W.D. Zhang, Sens. Actuators B: Chem. 2008 (2008) 403–408.
- [44] M. Sahal, B. Hariti, A. Ridah, M. Mollar, B. Mari, Microelectron. J. 39 (2008) 1425–1428.
- [45] P. Dhiman, J. Chand, A. Kumar, R.K. Kotnala, K.M. Batoo, M. Singh, J. Alloys Compd. 578 (2013) 235–241.
- [46] V.B. Patil, S.G. Pawar, S.L. Patil, J. Mater. Sci. Mater. Electron. 41 (2010) 335–357.
- [47] P.P. Sahay, R.K. Nath, S. Tewari, Cryst. Res. Technol. 42 (2007) 275–280.
- [48] S. Kant, S. Kalia, A. Kumar, J. Alloys Compd. 578 (2013) 249–256.
- [49] Y.B. Uum, B.S. Han, H.M. Lee, S.M. Hong, G.M. Kim, C.H. Rhee, Phys. Status Solidi C 4 (12) (2007) 4408–4411.
- [50] J. Rahamani, H.Z. Mousavi, Desalination 267 (2011) 256–260.
- [51] F.L. Zhang, J.C. Zhao, T. Shen, H. Hidaka, E. Pelizzetti, N. Serpone, Appl. Catal., B 15 (1998) 147–156.
- [52] C. Hu, Y.C. Tang, J.C. Yu, P.K. Wang, Appl. Catal., B 40 (2003) 131–140.
- [53] H.W. Bai, Z.Y. Liu, D.D. Sun, Chem. Phys. 13 (2011) 6205–6210.
- [54] T.L. Xu, Y. Cai, K.E.O. Shea, Environ. Sci. Technol. 41 (2007) 5471–5477.
- [55] C. Siriwig, N. Wetchakun, B. Inceesungvorn, D. Channei, T. Sanerjai, S. Phanichphant, Prog. Cryst. Growth. Ch. 58 (2–3) (2012) 145–163.
- [56] M.S. Hamdy, P. Nickel, I.H. Abd-Elmaksoud, H. Zhou, E.H. El-Mossalamy, A.O. Alyobi, S. Lynch, A. Nathan, G. Thornton, J. Photochem. Photobiol. A: Chem. 228 (2012) 1–7.
- [57] L.G. Devi, B.N. Murthy, S.G. Kumar, Mater. Sci. Eng. B 166 (2010) 1–6.
- [58] M.A. Nawii, S.Md. Zain, Appl. Surf. Sci. 258 (16) (2012) 6148–6157.
- [59] X. Cai, Y. Cai, H.Y.L. Li, F. Zhang, Y. Wang, J. Phys. Chem. Solids 74 (2013) 1196–1203.
- [60] M.M. Rashad, E.M. Elsayed, M.S. Al-Kotb, A.E. Shalan, J. Alloys Compd. 581 (2013) 71–78.
- [61] L. Song, J. Xiong, Q. Jiang, P. Du, H. Cao, X. Shao, Mater. Chem. Phys. 142 (2013) 77–81.
- [62] A.K. Gupta, A. Pal, C. Sahoo, Dyes Pigments 69 (2006) 224–232.
- [63] M. Radovic, Z. Saponjic, I.A. Jankovic, G. Ceric-Marjanovic, S.P. Ahrenkiel, Appl. Catal., B 136–137 (2013) 133–139.
- [64] V. Eskizeybek, F. Sari, H. Gulce, A. Gulce, A. Avci, Appl. Catal., B 119–120 (2012) 197–206.
- [65] Y. Khan, S.K. Durrani, M. Mehmood, J. Ahmad, M.R. Khan, S. Firdous, Appl. Surf. Sci. 257 (2010) 1756–1761.
- [66] S. Npohakundilognat, P. Nankorn, K. Sonjaipanich, N. Seetapan, S. Kaitkamjornwong, J. Appl. Polym. Sci. 114 (2009) 2564–2575.